

PAPER

# Fidelity spectrum: A tool to probe the property of a quantum phase<sup>\*</sup>

To cite this article: Wing Chi Yu and Shi-Jian Gu 2016 *Chinese Phys. B* **25** 030501

View the [article online](#) for updates and enhancements.

## You may also like

- [Adiabatic speedup via zero-energy-change control in a spin system](#)  
Li-Cheng Zhang, Feng-Hua Ren, Yi-Fei Chen et al.
- [Selective dynamical decoupling for quantum state transfer](#)  
H Frydrych, A Hoskovec, I Jex et al.
- [Quantum geometric machine learning for quantum circuits and control](#)  
Elija Perrier, Dacheng Tao and Chris Ferrie

# Fidelity spectrum: A tool to probe the property of a quantum phase\*

Wing Chi Yu<sup>†</sup> and Shi-Jian Gu

Department of Physics and ITP, The Chinese University of Hong Kong, Hong Kong, China

(Received 7 October 2015; revised manuscript received 2 December 2015; published online 20 January 2016)

Fidelity measures the similarity between two states and is widely adapted by the condensed matter community as a probe of quantum phase transitions in many-body systems. Despite its success in witnessing quantum critical points, information about the fine structure of a quantum phase one can get from this approach is still limited. Here, we proposed a scheme called fidelity spectrum. By studying the fidelity spectrum, one can obtain information about the characteristics of a phase. In particular, we investigated the spectra in the one-dimensional transverse-field Ising model and the two-dimensional Kitaev model on a honeycomb lattice. It was found that the spectra have qualitative differences in the critical and non-critical regions of the two models. From the distributions of them, the dominating  $k$  modes in a particular phase could also be captured.

**Keywords:** quantum phase transitions, quantum information, quantized spin models

**PACS:** 05.30.Rt, 64.70.Tg, 03.67.-a, 75.10.Jm

**DOI:** 10.1088/1674-1056/25/3/030501

## 1. Introduction

A quantum phase transition (QPT)<sup>[1,2]</sup> is driven by quantum fluctuations in the ground state of a many-body system. As an external parameter such as a magnetic field varies, the qualitative structure of the system's ground-state wavefunction exhibits an abrupt change across the quantum critical point. With this observation, researchers were motivated to use the fidelity, which is a concept borrowed from the quantum information theory, to study QPTs.<sup>[3,4]</sup>

Fidelity measures the similarity between two states. Mathematically, the static ground-state fidelity is defined as the magnitude of the overlap between two ground states differing from each other by a small value in the parameter space. Within one phase of the system, the two states have similar structures and thus the fidelity is close to unity. On the other hand, the ground states in distinct phases of the system are significantly different from each other. The fidelity is thus expected to show a sudden drop across the quantum critical point. The significance to use fidelity and its variations, such as fidelity susceptibility,<sup>[5,6]</sup> generalized fidelity susceptibility,<sup>[7]</sup> fidelity per site,<sup>[8,9]</sup> reduced fidelity,<sup>[10,11]</sup> operator fidelity,<sup>[12,13]</sup> and density-functional fidelity,<sup>[14]</sup> as a probe of QPTs have been testified in a number of condensed matter models (for a comprehensive review, please refer to Ref. [15]). Recently, an equality relating the fidelity susceptibility and the spectral function has been derived.<sup>[16]</sup> This makes the fidelity susceptibility to be directly measurable in experiments via neutron scattering or the angle-resolved photoemission spectroscopy (ARPES) techniques.

Although the fidelity can well witness a quantum critical point and provide us the critical exponents in continuous phase transitions,<sup>[17–20]</sup> the information about the nature and

the symmetry of a phase that one could obtain is limited. With the motivation to gain more insight about a quantum phase from the fidelity approach, we proposed the fidelity spectrum in this work. Recently, Gu *et al.*<sup>[21]</sup> and Sacramento *et al.*<sup>[22]</sup> also introduced the concepts of mode fidelity and fidelity spectrum, respectively, with similar motivations.

In Sacramento and his collaborators' proposal, the fidelity spectrum was defined through the fidelity operator  $F(\rho_1, \rho_2) = \text{Tr} \sqrt{\sqrt{\rho_1} \rho_2 \sqrt{\rho_1}}$ , where  $\rho_1$  and  $\rho_2$  are the reduced density matrices. The focus was on the partial state of the system. However, the global ground state of the system usually plays a role in a QPT. Especially in a topological QPT in which the global topological order of the system changes,<sup>[23]</sup> it may be insufficient to just consider the partial state of the system to characterize the quantum phase. At this point, we were motivated to define the fidelity spectrum using the global ground-state wavefunction of the system. We investigated the distributions of the spectra in the one-dimensional (1D) Ising model in a transverse field and the two-dimensional (2D) Kitaev model on a honeycomb lattice. The spectra were found to exhibit qualitative different behaviors in different regimes of the models. From the distributions of the spectra, one can determine the dominating  $k$  modes in a phase.

The paper is organized as follows. In Section 2, we established a general mathematical framework of the fidelity spectrum. The fidelity spectrum was studied in the 1D transverse-field Ising model, which exhibits a continuous QPT, and the honeycomb lattice Kitaev model, which exhibits a topological QPT. The results are discussed in Sections 3 and 4, respectively. Finally, a summary is given in Section 5.

\*Project supported by the Earmarked Research Grant from the Research Grants Council of HKSAR, China (Grant No. CUHK 401212).

<sup>†</sup>Corresponding author. E-mail: [wcyu@phy.cuhk.edu.hk](mailto:wcyu@phy.cuhk.edu.hk)

## 2. Fidelity spectrum

Consider a general form of Hamiltonian,

$$H(\lambda) = H_0 + \lambda H_I, \quad (1)$$

where  $H_I$  is the driving Hamiltonian and  $\lambda$  is an external driving parameter. Let  $\{|\Psi_n(\lambda)\rangle\}$  be a set of complete orthogonal eigen-basis of the Hamiltonian at  $\lambda$  with corresponding eigenenergies  $E_n(\lambda)$ , i.e.,  $H(\lambda)|\Psi_n(\lambda)\rangle = E_n(\lambda)|\Psi_n(\lambda)\rangle$ . Focusing on QPTs that are not induced by the ground-state level crossing, the ground state of the Hamiltonian in a finite system is non-degenerate. For a small change  $\delta\lambda$  in the external driving parameter, the non-degenerate perturbation theory could be applied. To the first-order correction, the perturbed ground state is

$$|\Psi_0(\lambda + \delta\lambda)\rangle = \frac{1}{\sqrt{1 + (\delta\lambda)^2 \chi_F}} |\Psi_0(\lambda)\rangle + \frac{\delta\lambda}{\sqrt{1 + (\delta\lambda)^2 \chi_F}} \sum_{n \neq 0} \frac{H_I^{n0}(\lambda) |\Psi_n(\lambda)\rangle}{E_0(\lambda) - E_n(\lambda)}, \quad (2)$$

where  $H_I^{nm}(\lambda) = \langle \Psi_n(\lambda) | H_I | \Psi_m(\lambda) \rangle$  and

$$\chi_F = \sum_{n \neq 0} \frac{|H_I^{n0}(\lambda)|^2}{[E_0(\lambda) - E_n(\lambda)]^2} \quad (3)$$

is the fidelity susceptibility.<sup>[5,6]</sup>

Consider the overlap

$$F_n(\lambda, \delta\lambda) = |\langle \Psi_n(\lambda) | \Psi_0(\lambda + \delta\lambda) \rangle|. \quad (4)$$

If the driving parameter  $\lambda$  is time-dependent, the overlap would be related to the quantum work distribution in quench dynamics.<sup>[24–26]</sup> For  $n = 0$ , the overlap is just the fidelity<sup>[3,4]</sup> as given by

$$F_0(\lambda, \delta\lambda) = |\langle \Psi_0(\lambda) | \Psi_0(\lambda + \delta\lambda) \rangle| = \frac{1}{\sqrt{1 + (\delta\lambda)^2 \chi_F}} \equiv \frac{1}{p}. \quad (5)$$

For  $n \neq 0$ , we have

$$F_{n \neq 0}(\lambda, \delta\lambda) = |\langle \Psi_{n \neq 0}(\lambda) | \Psi_0(\lambda + \delta\lambda) \rangle| = \sqrt{1 - \frac{1}{p^2} M_n(\lambda)}, \quad (6)$$

where

$$M_n(\lambda) = \frac{1}{\chi_F} \left| \frac{H_I^{n0}(\lambda)}{E_0(\lambda) - E_n(\lambda)} \right|. \quad (7)$$

The fidelity spectrum we discussed in this work is defined by the set  $\{M_n(\lambda)\}$ , which is independent of  $\delta\lambda$ .

Physically, the fidelity spectrum tells us how much the ground state of the final Hamiltonian comes from different eigenstates of the initial Hamiltonian. When the system is under an external perturbation  $\delta\lambda H_I$ , the perturbed ground state

is in general a superposition of the eigenstates of the unperturbed Hamiltonian. The contribution from the ground state is given by the fidelity while the contribution from the  $n$ -th excited state of the original Hamiltonian is governed by  $M_n$ . As one can see from Eq. (7), the fidelity spectrum depends on the scattering amplitude of the driving Hamiltonian and also the energy gap between the ground state and the excited state. By investigating the distribution of  $\{M_n\}$ , we expect to gain information about the modes that are dominating in a quantum phase.

To have a quantitative description of the distribution of  $\{M_n\}$ , we introduce a quantity

$$S_F(\lambda) = \sum_{n \neq 0} -|M_n(\lambda)|^2 \ln |M_n(\lambda)|^2. \quad (8)$$

Since  $M_n$  has a probability interpretation of the final ground state being contributed from an excited state of the original Hamiltonian and it is normalized, i.e.,  $\sum_{n \neq 0} |M_n(\lambda)|^2 = 1$ ,  $S_F$  can be regarded as an analogy to the Shannon entropy characterizing the distribution. The more spread the distribution of  $\{M_n\}$  is, the larger  $S_F$  is expected. While for a less spread distribution,  $S_F$  would be smaller.

## 3. One-dimensional transverse-field Ising model

The 1D transverse-field Ising model is one of the simplest many-body systems, which is exactly solvable and exhibits a QPT.<sup>[27–31]</sup> The Hamiltonian of the model is given by

$$H_{\text{Ising}} = - \sum_{j=1}^N (\sigma_j^x \sigma_{j+1}^x + h \sigma_j^z), \quad (9)$$

where  $\sigma_j^\kappa$ , with  $\kappa = x, y, z$ , is the Pauli matrix,  $N$  is the number of spins, and  $h$  characterizes the strength of the external field in the unit of the coupling constant. Periodic boundary condition is adapted here.

The model's Hamiltonian can be diagonalized through standard procedure using the Jordan–Wigner transformation, Fourier transformation, and Bogoliubov transformation.<sup>[1]</sup> After these transformations, equation (9) becomes

$$H_{\text{Ising}} = \sum_k \varepsilon_k(h) (2b_k^\dagger b_k - 1), \quad (10)$$

where

$$\varepsilon_k(h) = \sqrt{1 - 2h \cos k + h^2}, \quad (11)$$

and  $k$  is the momentum wavevector with values of  $(2m + 1)\pi/N$  for  $m = -N/2, -N/2 + 1, \dots, N/2 - 1$ . In the thermodynamic limit, the system is gapless only at  $h = 1$  and gapped for other values of  $h > 0$ . A continuous QPT takes place at  $h_c = 1$ . For  $0 \leq h < 1$ , the system is a ferromagnet, while it is paramagnetic for  $h > 1$ . Recently, the system has been experimentally realized by tuning a strong transverse magnetic field in  $\text{CoNb}_2\text{O}_6$  (cobalt niobate). By detecting the low-energy excitation in neutron scattering experiment, a continuous QPT was observed in the material.<sup>[32]</sup>

To investigate the fidelity spectrum in Eq. (7), we take the driving Hamiltonian as

$$H_I = - \sum_{j=1}^N \sigma_j^z. \quad (12)$$

The fidelity spectrum was calculated to be

$$M_k(h) = \frac{1}{\sqrt{\chi_F}} \frac{\sin k}{2\varepsilon_k^2}, \quad (13)$$

where  $k$  is used as an index to characterize an excited state in which a pair of quasiparticles with momentum  $k$  and  $-k$  is created. The fidelity susceptibility is given by<sup>[33]</sup>

$$\chi_F = \frac{N^2}{16h^2} \frac{h^N}{(h^N + 1)^2} + \frac{N}{16h^2} \frac{h^N - h^2}{(h^N + 1)(h^2 - 1)}. \quad (14)$$

Our main target is to investigate the distribution of the fidelity spectrum, which is closely related to the probability distribution of the  $k$  mode excitations discussed in the context of quench dynamics.<sup>[34,35]</sup>

Figure 1 shows the distribution of  $M_k$  over the  $k$ -space for various values of  $h$ . From the figure, we see that for  $h$  away from the critical point, the distribution of the fidelity spectrum is more widely spread. However, at the critical field  $h = 1$ , the distribution is dominated by the zero-th mode and shows an exponential decaying trend away from this mode. One may understand this behavior by referring to Eq. (7) and noting that the energy gap between the ground state and the first excited state vanishes at the critical point.

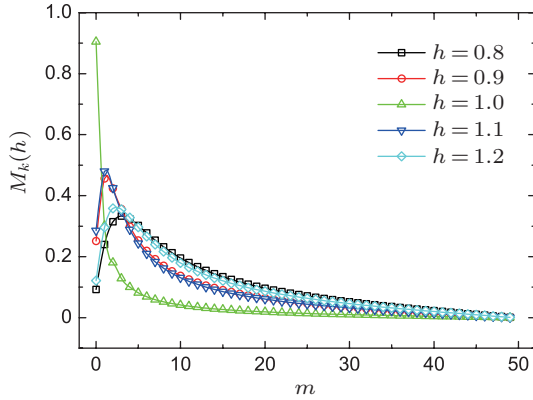
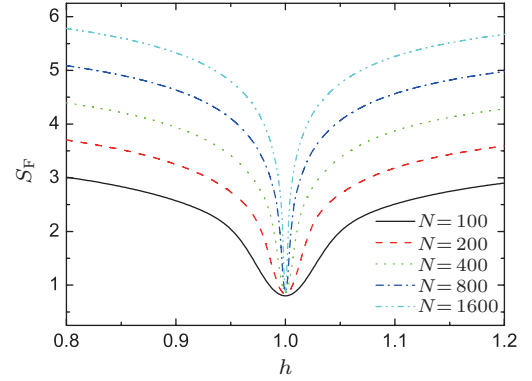


**Fig. 1.** (color online) A plot of  $M_k$  in Eq. (13) distributed over the  $k$ -space for the 1D transverse-field Ising model. Here  $N = 100$  and  $k = (2m + 1)\pi/N$ . Only positive  $k$ 's are shown.

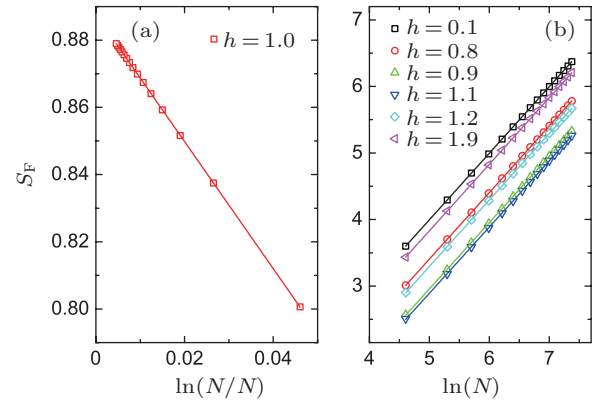
Quantitatively, we can also obtain the dominating mode by considering  $dM_k/dk = 0$  which gives  $\cos k = 2h/(1 + h^2)$ . For  $h = 1$ ,  $k = 0$  is a solution to the equation. However, note that for  $N$  is even,  $k = (2m + 1)\pi/N$  and the  $k = 0$  mode is not allowed in a finite system. Instead,  $M_k$  peaks at  $k = \pi/N$ , which in turn tends to zero as  $N$  tends to infinity.

Figure 2 shows a plot of  $S_F$  as a function of  $h$  for various system sizes. At  $h = 1$ , the fidelity spectrum is dominated by the zero-th mode.  $S_F$  is thus a minimum as expected. On the

other hand, the fidelity spectra in the non-critical region are more spread and  $S_F$  becomes larger.



**Fig. 2.** (color online)  $S_F$  as a function of  $h$  for various system size in the 1D transverse-field Ising model.



**Fig. 3.** (color online) (Left) The scaling behavior of  $S_F$  at the critical point of the 1D transverse-field Ising model. The straight line shows the linear fit of  $-1.89 \ln N/N + 0.89$ . (Right) The scaling behavior of  $S_F$  in the non-critical region. The slope of the straight line is 1 (maximum error =  $\pm 0.001$ ).

In addition, a point worth noting from the figure is that  $S_F$  is insensitive to the system size at the critical point while it shows a non-trivial scaling behavior with  $N$  for  $h \neq 1$ . For  $h = 1$ , the size dependence of  $S_F$  can be obtained analytically. Putting Eq. (13) into Eq. (8), we have

$$\begin{aligned} S_F &\simeq -N \int_{\pi/N}^{\pi(N-1)/N} \frac{1}{4\chi_F k^2} \ln \left[ \frac{1}{4\chi_F k^2} \right] dk, \\ &\sim \frac{N}{\chi_F} \left[ N \ln \left( \frac{\chi_F}{N^2} \right) - \ln(\chi_F) + N \right]. \end{aligned} \quad (15)$$

From Eq. (14),  $\chi_F(h = 1) = N(N - 1)/32$  and we obtain

$$S_F \sim AN^0 + \frac{B}{N} \ln \frac{1}{N}, \quad (16)$$

where  $A$  and  $B$  are some constants independent of  $N$ . In the limit where  $N \rightarrow \infty$ ,  $S_F$  tends to a constant.

Figure 3 shows a plot of the scaling dependence of  $S_F$  with the system size. From linear fitting, we obtain

$$S_F \sim \begin{cases} 1.89 \frac{1}{N} \ln \frac{1}{N} + 0.89, & \text{for } h = 1, \\ 1.00 \ln N, & \text{for } h \neq 1. \end{cases} \quad (17)$$

In the thermodynamic limit,  $S_F$  tends to a constant at the critical point as expected from the analytical analysis above. On the other hand,  $S_F$  shows a logarithmic divergence away from the critical point. This implies that fidelity spectrum becomes more and more dispersive as the system size increases.

#### 4. The Kitaev model on a honeycomb lattice

The Kitaev model was first introduced by Kitaev to study anyonic statistics.<sup>[36]</sup> The ground state of the model can be exactly obtained and it is found to possess a topological QPT.<sup>[36,37]</sup> Its ground-state phase diagram consists of gapless phases with non-Abelian anyon excitations and gapped phases with Abelian anyon excitations. As an exactly solvable 2D model exhibiting such an interesting phase diagram, the Kitaev model and its extensions have been intensively studied in the field of condensed matter physics (for examples, please see Refs. [38]–[42]). Besides, the model also captured much attention in the field of quantum information processing for its potential to realize the fault-tolerant quantum computation.<sup>[43]</sup>

The model consists of  $1/2$  spins located at the vertices of a honeycomb lattice. They are interacting with the nearest neighbors through three types of bonds, namely,  $x$ ,  $y$ , and  $z$  bond, depending on their directions (see Fig. 4). The Hamiltonian reads<sup>[36]</sup>

$$H_{\text{Kitaev}} = -J_x \sum_{x\text{-bond}} \sigma_j^x \sigma_k^x - J_y \sum_{y\text{-bond}} \sigma_j^y \sigma_k^y - J_z \sum_{z\text{-bond}} \sigma_j^z \sigma_k^z, \quad (18)$$

where  $j, k$  denote the vertex of the corresponding bonds.  $J_x$ ,  $J_y$ , and  $J_z$  are dimensionless coupling constants in  $x$ ,  $y$ , and  $z$  directions, respectively.

Consider the plaquette labeled as  $p$  in Fig. 4. The operator  $W_p = \sigma_1^x \sigma_2^y \sigma_3^z \sigma_4^x \sigma_5^y \sigma_6^z$  commutes with the Hamiltonian for all  $p$ . Obviously,  $W_p$  of different plaquettes also commute. Therefore, the Hilbert space can be divided into subspaces with  $w_p = \pm 1$  for each plaquette. The ground state lies in the subspace in which all  $w_p$  are equal to one. This is the key feature that makes an exact solution to the model possible.<sup>[36,37]</sup>

The Hamiltonian in Eq. (18) can be diagonalized by two different methods.<sup>[36,37]</sup> Following the approach introduced by Chen *et al.* in Ref. [37], the honeycomb lattice is first deformed into a topologically equivalent brick-wall lattice by stretching the lattice horizontally (see Fig. 4). Defining the Jordan–Wigner transformation as

$$\sigma_{n,m}^z = 2c_{n,m}^{\dagger (s)} c_{n,m}^{(s)} - 1, \quad (19)$$

$$\sigma_{n,m}^+ = 2c_{n,m}^{\dagger (s)} \left[ \prod_{n'=0}^{\tilde{N}-1} \prod_{m'=0}^{m-1} \sigma_{n',m'}^z \right] \left[ \prod_{n'=0}^{n-1} \sigma_{n',m}^z \right], \quad (20)$$

$$\sigma_{n,m}^- = 2c_{n,m}^{(s)} \left[ \prod_{n'=0}^{\tilde{N}-1} \prod_{m'=0}^{m-1} \sigma_{n',m'}^z \right] \left[ \prod_{n'=0}^{n-1} \sigma_{n',m}^z \right], \quad (21)$$

where  $n$  and  $m$  are the column and row indices, respectively.  $\tilde{N}$  is the number of sites in each row, and  $c_{n,m}$  and  $c_{n,m}^{\dagger}$  are fermion annihilation and creation operators, respectively. The superscript  $s = b, w$  denotes the black and white sites, respectively.

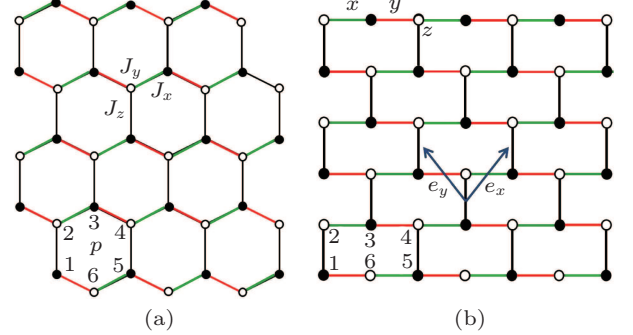


**Fig. 4.** (color online) (a) A sketch of the Kitaev model on a honeycomb lattice. The lattice can be divided into two equivalent triangular sublattices denoted by the black and white dots. (b) A deformation of the honeycomb lattice on the left into a topologically equivalent brick-wall lattice.  $e_x$  and  $e_y$  are the unit vectors connecting the mid-point of the  $z$  bonds.

Introducing the Majorana fermion operators

$$A_{n,m}^{(w)} = -i(c_{n,m}^{(w)} - c_{n,m}^{\dagger (w)}), \quad (22)$$

$$B_{n,m}^{(w)} = c_{n,m}^{(w)} + c_{n,m}^{\dagger (w)}, \quad (23)$$

$$A_{n,m}^{(b)} = c_{n,m}^{(b)} + c_{n,m}^{\dagger (b)}, \quad (24)$$

$$B_{n,m}^{(b)} = -i(c_{n,m}^{(b)} - c_{n,m}^{\dagger (b)}), \quad (25)$$

the Hamiltonian is then transformed into

$$H_{\text{Kitaev}} = -J_x \sum_{n+m=\text{odd}} iA_{n,m}^{(w)} A_{n+1,m}^{(b)} - J_y \sum_{n+m=\text{even}} (-i)A_{n,m}^{(b)} A_{n+1,m}^{(w)} - J_z \sum_{n+m=\text{even}} (i\hat{\alpha}_r)A_{n,m}^{(b)} A_{n,m+1}^{(w)}, \quad (26)$$

where  $r$  is the coordinate to the mid-point of a  $z$  bond connecting the black and white sites at  $(n, m)$  and  $(n, m+1)$ .  $\hat{\alpha}_r = iB_{n,m}^{(b)} B_{n,m+1}^{(w)}$  and is related to  $W_p$  by  $W_p = \hat{\alpha}_{12} \hat{\alpha}_{45}$ . By taking all  $\alpha_r = 1$ , the Hamiltonian becomes quadratic and can be diagonalized through Bogoliubov transformation into

$$H_{\text{Kitaev}} = \sum_{\mathbf{k}} \sqrt{\varepsilon_{\mathbf{k}}^2 + \Delta_{\mathbf{k}}^2} \left( b_{\mathbf{k}}^{\dagger} b_{\mathbf{k}} - \frac{1}{2} \right), \quad (27)$$

where

$$\varepsilon_{\mathbf{k}} = 2J_z - 2J_x \cos k_x - 2J_y \cos k_y, \quad (28)$$

$$\Delta_{\mathbf{k}} = 2J_x \sin k_x + 2J_y \sin k_y, \quad (29)$$

$b_{\mathbf{k}}$  and  $b_{\mathbf{k}}^{\dagger}$  is another set of fermionic operators satisfying the usual anti-commutation relations.  $k_{x(y)}$  is the momentum wavevector with values of  $(2m_{x(y)} + 1)\pi/L$  for  $m_{x(y)} = -L/2, \dots, L/2 - 1$ .



For

$$\begin{cases} |J_z| \leq |J_x| + |J_y|, \\ |J_x| \leq |J_y| + |J_z|, \\ |J_y| \leq |J_z| + |J_x|, \end{cases} \quad (30)$$

the system is gapless in the thermodynamic limit. In this gapless phase, the excitation is described by non-Abelian anyons. For the coupling constants outside the range given by Eq. (30), the system is in a gapped phase and obeys Abelian anyonic statistics. In the intermediate regime, a topological quantum phase transition takes place. A schematic phase diagram on the  $J_x + J_y + J_z = 1$  plane is shown in the inset of Fig. 6.

To calculate the ground-state fidelity spectrum, let us consider varying  $J_z$  along the  $J_x = J_y$  line on the  $J_x + J_y + J_z = 1$

plane (see the red dashed line in the inset of Fig. 6). The interaction Hamiltonian is given by

$$H_I = \frac{1}{2} \sum_{x\text{-bond}} \sigma_j^x \sigma_k^x + \frac{1}{2} \sum_{y\text{-bond}} \sigma_j^y \sigma_k^y - \sum_{z\text{-bond}} \sigma_j^z \sigma_k^z. \quad (31)$$

The fidelity spectrum was found to be

$$M_{\mathbf{k}}(J_z) = \frac{1}{\sqrt{\chi_F}} \frac{(\sin k_x + \sin k_y)}{4(\epsilon_{\mathbf{k}}^2 + \Delta_{\mathbf{k}}^2)}, \quad (32)$$

and the fidelity susceptibility can be calculated by<sup>[44]</sup>

$$\chi_F = \frac{1}{16} \sum_{\mathbf{k}} \left( \frac{\sin k_x + \sin k_y}{\epsilon_{\mathbf{k}}^2 + \Delta_{\mathbf{k}}^2} \right)^2. \quad (33)$$

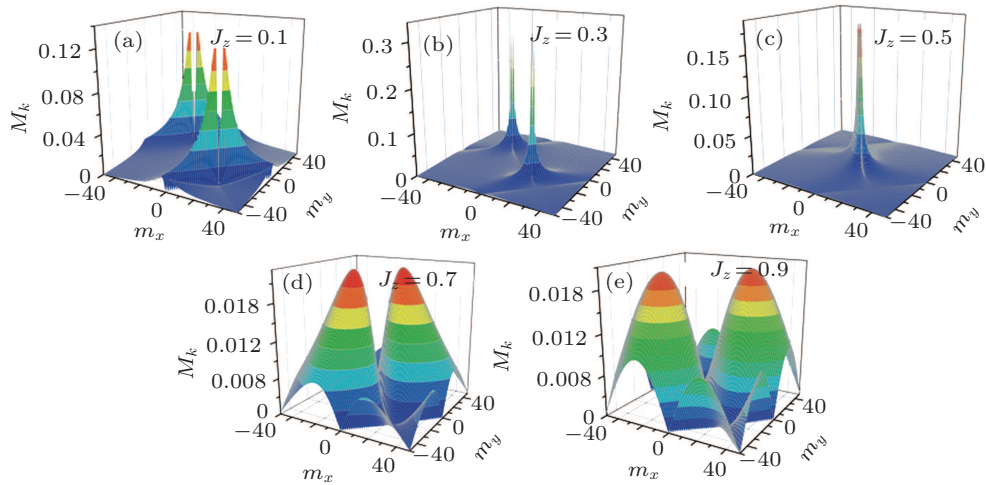


**Fig. 5.** (color online) 3D plots of the distributions of  $M_{\mathbf{k}}$  over the  $\mathbf{k}$  space for (a)  $J_z = 0.1$ , (b) 0.3, (c) 0.5, (d) 0.7, (e) 0.9 in the Kitaev model. Here  $k_x = (2m_x + 1)\pi/L$  and  $k_y = (2m_y + 1)\pi/L$ , and  $L = 100$ .

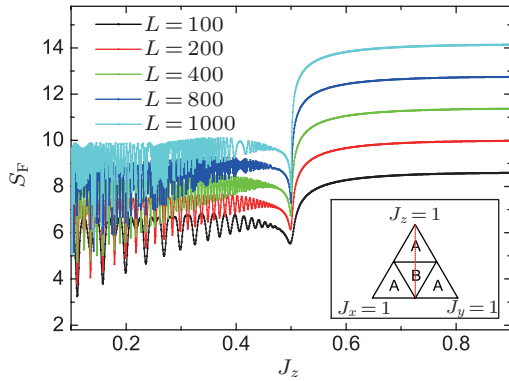


**Fig. 6.** (color online)  $S_F$  as a function of  $J_z$  for various system size. The lines represent the cases for  $L = 100, 200, 400, 800$ , and  $1600$ , respectively, when going upward. The inset shows a schematic phase diagram on the  $J_x + J_y + J_z = 1$  plane of the Kitaev model. The A phase is gapped, while the B phase is gapless. A topological QPT takes place at  $J_z = 0.5$  along the  $J_x = J_y$  line (as indicated by the dashed line).

The distribution of  $M_{\mathbf{k}}$  over the  $\mathbf{k}$  space for  $J_z = 0.1, 0.3, 0.5, 0.7, 0.9$  are shown in the 3D plots in Fig. 5. In the gapless phase where  $J_z < 0.5$ , the fidelity spectrum consists of four peaks. These peaks become more concentrated to the zone center as the value of  $J_z$  approaches the critical point

at  $J_z = 0.5$ . While in the gapped phase ( $J_z > 0.5$ ), the spectrum becomes more dispersive and there is no singular peak.

The behavior of the fidelity spectrum in the gapless phase of the Kitaev model is similar to that at the critical point of the Ising model in which the energy gap vanishes. When the system is gapless in the energy spectrum, the ground state is readily excited to other states. From the peaks in the fidelity spectrum, one can immediately realize which modes' contributions are the largest for various values of  $J_z$ .

Figure 6 shows a plot of  $S_F$  in Eq. (8) as a function of  $J_z$  for various system sizes. From the figure, we see that  $S_F$  for  $J_z < 0.5$  is smaller than that for  $J_z > 0.5$ . This echoes the fact that the fidelity spectrum in the gapless phase is less dispersive than that in the gapped phase.

Moreover,  $S_F$  in the gapless phase is an oscillating function of  $J_z$ . This feature comes from the periodic level-crossing occurred in the excited states of the system. The oscillation patterns are magnified in Fig. 7. As the system size increases, the number of oscillation cycles increases. From the linear fitting on the right panel in Fig. 7, we find that

$$\omega_0 \sim L^{0.991}, \quad (34)$$

where  $\omega_0$  is the frequency of oscillation. From Fig. 6, we also recognize that  $S_F$  exhibits some non-trivial scaling behaviors. It increases with the system size. Its scaling behavior is analyzed in Fig. 8. For  $J_z < 0.5$ ,  $S_F$  is oscillating and we take the values enclosed by the upper envelopes to perform the scaling analysis. By linear fitting, we find that

$$S_F \sim \begin{cases} (1.12 \pm 0.04) \ln L, & \text{for } J_z < 0.5, \\ (0.78 \pm 0.01) \ln L, & \text{for } J_z = 0.5, \\ (2 \pm 10^{-6}) \ln L, & \text{for } J_z > 0.5. \end{cases} \quad (35)$$

Interestingly, like the Ising model, the pre-factor of the size dependence of  $S_F$  in the gapped region is also equal to unity. If we express the scaling behaviors in the two models both in terms of  $N$ , we have

$$S_F \sim \ln N, \quad (36)$$

in a gapped region. Whether this relation is general for other gapped phases in many-body systems or not still needs further exploration.

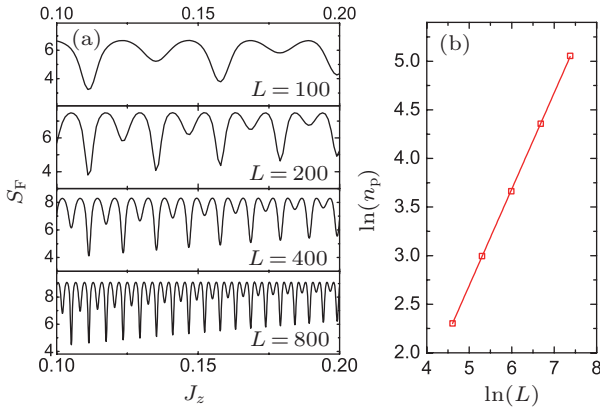


**Fig. 7.** (color online) (a) Oscillating pattern of  $S_F$  in the gapless phase. (b) Size dependence of the number of peaks ( $n_p$ ) in  $S_F$  in the gapless phase. The slope of the straight line is  $0.991 \pm 0.004$ .

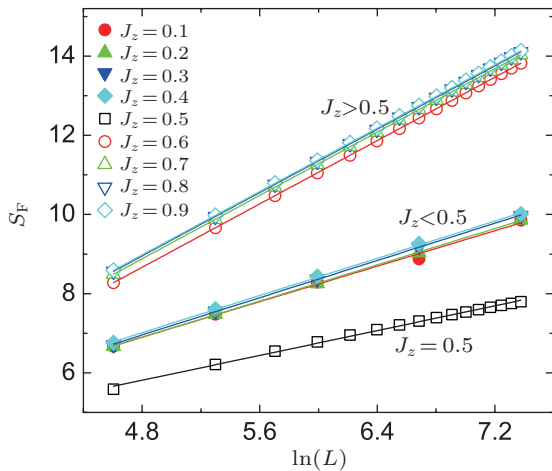


**Fig. 8.** (color online) Scaling behavior of  $S_F$  for various values of  $J_z$ . The straight lines are the linear fitting of the data points.

## 5. Summary

In summary, we investigated the fidelity spectra in the 1D transverse-field Ising model which exhibits a continuous QPT, and in the 2D honeycomb lattice Kitaev model which exhibits a topological QPT. We found that the fidelity spectrum shows qualitatively different behaviors in different phases of the model. A common feature about the spectrum is that the distribution is dominated by certain  $k$  modes in the gapless region while it is more dispersive in the gapped region.

To characterize the distribution of the fidelity spectrum quantitatively, we introduced the quantity  $S_F$  in analogy to the Shannon entropy. It was found that at the critical point of the Ising model,  $S_F \sim \ln N/N$  while it scales with  $\ln N$  in the non-critical region. The latter scaling behavior also holds for the Kitaev model. The universality of the relation in Eq. (36) requires further exploration.

## Acknowledgment

W C Yu thank H Q Lin for the helpful discussion and W L You for the useful feedback on the manuscript.

## References

- [1] Sachdev S 1999 *Quantum Phase Transitions* (Cambridge: Cambridge University Press)
- [2] Carr L 2011 *Understanding Quantum Phase Transitions* (Boca Raton: CRC Press)
- [3] Quan H T, Song Z, Liu X F, Zanardi P and Sun C P 2006 *Phys. Rev. Lett.* **96** 140604
- [4] Zanardi P and Paunković N 2006 *Phys. Rev. E* **74** 031123
- [5] You W L, Li Y W and Gu S J 2007 *Phys. Rev. E* **76** 022101
- [6] Zanardi P, Giorda P and Cozzini M 2007 *Phys. Rev. Lett.* **99** 100603
- [7] You W L and He L 2015 *J. Phys.: Condens. Matter* **27** 205601
- [8] Zhou H Q and Barjaktarević J P 2008 *J. Phys. A* **41** 412001
- [9] Zhou H Q, Orús R and Vidal G 2008 *Phys. Rev. Lett.* **100** 080601
- [10] Gorin T, Prosen T, Seligman T H and Žnidarič M 2006 *Phys. Rep.* **435** 33
- [11] Paunković N, Sacramento P, Nogueira P, Vieira V and Dugave V 2008 *Phys. Rev. A* **77** 052302
- [12] Lu X M, Sun Z, Wang X and Zanardi P 2008 *Phys. Rev. A* **78** 032309
- [13] Wang X, Sun Z and Wang Z D 2009 *Phys. Rev. A* **79** 012105
- [14] Gu S J 2009 *Chin. Phys. Lett.* **26** 026401
- [15] Gu S J 2010 *Int. J. Mod. Phys. B* **24** 4371
- [16] Gu S J and Yu W C 2014 *Europhys. Lett.* **108** 20002
- [17] Venuti L C and Zanardi P 2007 *Phys. Rev. Lett.* **99** 095701
- [18] Gu S J, Kwok H M, Ning W Q and Lin H Q 2008 *Phys. Rev. B* **77** 245109
- [19] Albuquerque A F, Alet F, Sire C and Capponi S 2010 *Phys. Rev. B* **81** 064418
- [20] Rams M and Damski B 2011 *Phys. Rev. Lett.* **106** 055701
- [21] Gu S J, Yu W C and Lin H Q 2013 *Int. J. Mod. Phys. B* **27** 1350106
- [22] Sacramento P D, Paunković N and Vieira V R 2011 *Phys. Rev. A* **84** 062318
- [23] Wen X G 2004 *Quantum Field Theory of Many-body Systems* (New York: Oxford University)
- [24] Tasaki H 2000 arXiv:0009244[cond-mat]
- [25] Kurchan J 2007 *J. Stat. Mech. Theor. Exp.* **2007** P07005
- [26] Mukamel S 2003 *Phys. Rev. Lett.* **90** 170604
- [27] Pfeuty P 1970 *Ann. Phys.* **57** 79
- [28] Elliott R J, Pfeuty P and Wood C 1970 *Phys. Rev. Lett.* **25** 443
- [29] Jullien R, Pfeuty P, Fields J N and Doniach S 1978 *Phys. Rev. B* **18** 3568
- [30] Barouch E and McCoy B M 1970 *Phys. Rev. A* **2** 1075
- [31] Barouch E and McCoy B M 1971 *Phys. Rev. A* **3** 786
- [32] Coldea R, Tennant D, Wheeler E, Wawrzynska E, Prabhakaran D, Telling M, Habicht K, Smeibidl P and Kiefer K 2010 *Science* **327** 177

- [33] Damski B 2013 *Phys. Rev. E* **87** 052131
- [34] Deng S, Ortiz G and Viola L 2011 *Phys. Rev. B* **83** 094304
- [35] Rams M and Damski B 2011 *Phys. Rev. A* **84** 032324
- [36] Kitaev A 2006 *Ann. Phys. (N.Y.)* **443** 312
- [37] Chen H D and Nussinov Z 2008 *J. Phys. A: Math. Theor.* **41** 075001
- [38] Feng X Y, Zhang G M and Xiang T 2007 *Phys. Rev. Lett.* **98** 087204
- [39] Lee D H, Zhang G M and Xiang T 2007 *Phys. Rev. Lett.* **99** 196805
- [40] Baskaran G, Mandal S and Shankar R 2007 *Phys. Rev. Lett.* **98** 247201
- [41] Mondal S, Sen D and Sengupta K 2008 *Phys. Rev. B* **78** 045101
- [42] Shi X F, Yu Y, You J Q and Nori F 2009 *Phys. Rev. B* **79** 134431
- [43] Kitaev A 2003 *Ann. Phys.* **303** 2
- [44] Yang S, Gu S J, Sun C P and Lin H Q 2008 *Phys. Rev. A* **78** 012304